

See discussions, stats, and author profiles for this publication at: <https://www.researchgate.net/publication/262907616>

Niobium: Activator and Stabilizer for a Copper-Based Deacon Catalyst

ARTICLE in CHEMCATCHEM · JANUARY 2014

Impact Factor: 4.56 · DOI: 10.1002/cctc.201300697

CITATIONS

4

READS

19

6 AUTHORS, INCLUDING:



Reinhard Schomäcker

Technische Universität Berlin

284 PUBLICATIONS 3,587 CITATIONS

SEE PROFILE



Klaus Stöwe

Technische Universität Chemnitz

99 PUBLICATIONS 1,072 CITATIONS

SEE PROFILE



Wilhelm F Maier

Universität des Saarlandes

134 PUBLICATIONS 3,517 CITATIONS

SEE PROFILE

Niobium: Activator and Stabilizer for a Copper-Based Deacon Catalyst

Markus Hammes,^[a] Hary Soerijanto,^[b] Reinhard Schomäcker,^[b] Martin Valtchev,^[a] Klaus Stöwe,^[a] and Wilhelm F. Maier^{*[a]}

A highly active Cu-based Deacon catalyst with an enhanced lifetime was developed by combining two corrosion-resistant high-throughput reactor setups in this combinatorial study. Catalyst activities were studied in a sequential 10-fold reactor equipped with online MS. For accelerated catalyst ageing studies, a parallel 10-fold reactor was used. The starting point was a CuTi mixed-metal oxide found in former discovery investigations. As development criteria, catalyst stability and HCl con-

version were selected. The amount of Cu in the CuTi catalysts were analyzed before and after the ageing process by X-ray fluorescence spectroscopy. Dopant elements were selected that are reported to form oxides with a high corrosion resistance against gaseous HCl. Our study revealed that doping with 1 mol% Nb reduced the Cu leaching during the reaction. Furthermore, the activation energy was decreased by Nb, which enhanced the chlorine production.

Introduction

Chlorine is an essential reagent in the chemical industry for the manufacture of products used in our everyday lives such as polymers, materials, and drugs. However, Cl₂ is produced almost exclusively by chloralkali electrolysis. This process is dominated by its high energy consumption that leads to high production costs and, consequently, to huge CO₂ emissions.^[1] Therefore, the chlorine industry is continuously spending time and effort to increase process efficiency and sustainability. One approach is the recycling of the common byproduct HCl, which is formed, for example, during the production of polyurethanes or polycarbonates through intermediate phosgenation. The options for chlorine recovery from HCl are electrolysis and the heterogeneously catalyzed oxidation of HCl in the so-called Deacon reaction. Electrolysis is easy to handle for the manufacturer; however, the energy consumption of this process is still a drawback,^[2] whereas the Deacon process with a heterogeneous Ru-based catalyst uses 80% less energy than HCl electrolysis.^[3]

The Deacon process was originally based on heterogeneous Cu catalysts that tend to slowly evaporate because of the low melting point and volatility of CuCl formed during the process. As a result of the HCl/Cl₂/H₂O atmosphere, Deacon process conditions are a real challenge for all materials in contact with the gaseous atmosphere, especially the catalysts. The lack of


sufficient catalyst lifetime has impeded the industrial application of most catalysts. At the beginning of this century, Sumitomo patented and reported a RuO₂-based catalyst supported on TiO₂ (rutile) with a high activity and outstanding lifetime for the Deacon process.^[3–5] This catalyst triggered increasing interest in heterogeneously catalyzed HCl oxidation. Subsequently, Bayer patented a RuO₂ catalyst supported on SnO₂ (cassiterite).^[6–8] The beneficial properties of RuO₂ were discussed in many articles, in particular, the recent reviews of Pérez-Ramírez et al. and Over are recommend for further reading.^[2,9,10]

Recently, Amrute et al. and Kondratenko et al. have demonstrated highly active RuO₂-based catalysts, which have a four- to 12-fold lower Ru content without compromising the stability.^[11,12] Nevertheless, there is still a need for alternative catalysts. During various investigations Ce, Cr, Cu, Mn, U, and V proved to be promising active elements for the Deacon process.^[13–21] The most suitable catalysts were Ce- and Cu-based materials. CeO₂ is remarkably stable under Deacon reaction conditions; however, it requires high temperatures for an adequate chlorine yield.^[13] In contrast, Cu-based catalysts yield more chlorine than Ce materials at temperatures below 400 °C. However, these Cu-based catalysts need to be stabilized against bulk chlorination, which leads to vaporization of copper chlorides and finally to the loss of the active phase. The catalyst lifetime is enhanced by doping with alkali metals such as K. The stabilization effect is related to the formation of potassium copper chlorides that have a lower vapor pressure than pure copper chlorides.^[16] Another approach is to stabilize Cu ions in specific crystal lattices that have a high resistance against bulk chlorination, such as the delafossite crystal structure.^[17,18]

In previous articles we reported a high-throughput setup equipped with an online mass spectrometer with a high resistance to corrosion as an analytical tool and its use in the search

[a] Dr. M. Hammes, M. Valtchev, Prof. Dr. K. Stöwe, Prof. Dr. W. F. Maier
Lehrstuhl für Technische Chemie
Saarland University
66123 Saarbrücken (Germany)

[b] Dr. H. Soerijanto, Prof. Dr. R. Schomäcker
Department of Chemistry
Technical University of Berlin
10623 Berlin (Germany)

 Supporting information for this article is available on the WWW under <http://dx.doi.org/10.1002/cctc.201300697>.

for alternative Deacon catalysts.^[22,23] The exceptional benefit of our setup is the possibility of an accelerated long-term ageing study of 10 potential catalysts in parallel under conditions close to those of the industrial process. Therefore, we are able to identify hits with significant relevance for industrial applications. Furthermore, MS-based mass balances enabled us to distinguish between bulk chlorination and heterogeneously catalyzed gas-phase HCl oxidation. During our screening, over 500 different Ce, Cr, Co, Cu, Fe, La, Mn, Ni, and Zn binary and highly diverse, doped Ti and Sn mixed-metal oxides were tested.^[24] Through data mining, a relationship between the stability data of pure metal oxides under chlorinating conditions accessible from the literature [mainly chlorination and vaporization temperature of metal halides (T_4)] and binary mixed-metal oxide Deacon stability was observed. Additionally, a Ru-doped Co spinel was discovered that competes with the well-known rutile systems.^[22] Apart from this catalyst, a CuTi mixed-metal oxide with outstanding HCl conversion was found. However, initially it showed the drawback of rapid deactivation.

We report here the development of stabilized Cu-based catalysts for the Deacon reaction based on our previous results.^[22] In this study a sequential 10-fold reactor for catalytic testing was supplemented by a parallel 10-fold reactor for ageing studies under reaction conditions.

Results and Discussion

During our screening for alternative Deacon catalysts, apart from a ZrRuCo mixed-metal oxide, the most promising candidate was $\text{Cu}_{10}\text{Ti}_{90}\text{O}_x$.^[24] The mixed oxide revealed a space time yield (STY) of $3.00 \text{ g}_{\text{Cl}_2} \text{ h}^{-1} \text{ g}_{\text{catalyst}}^{-1}$ at $T=410^\circ\text{C}$ to achieve equilibrium gas composition. In contrast, for pure CuO, a STY of only $0.72 \text{ g}_{\text{Cl}_2} \text{ h}^{-1} \text{ g}_{\text{catalyst}}^{-1}$ at $T=450^\circ\text{C}$ was reported.^[25] Therefore, we decided to try once more to improve the traditional Cu catalyst based on the concept of evolution by variation and selection.^[26] The objective of the subsequent high-throughput optimization cycles reported herein was to achieve a higher low-temperature activity and improved long-term stability of the catalyst based on Cu and Ti.

Screening the first generation

The first aim was to improve the activity of the $\text{Cu}_{10}\text{Ti}_{90}\text{O}_x$ catalyst at temperatures lower than 410°C . The stability of the Cu-doped catalysts was enhanced by decreasing the light-off temperature as copper chlorides begin to sublime off the catalyst bed at temperatures higher than 350°C .^[27] The CuTi mixed oxide was initially doped with 2 mol% of the following 20 elements (E): Al, B, Ca, Ce, Co, Ge, Hf, K, La, Mg, Na, Nb, Ni, Sc, Si, Sn, Ta, W, Y, and Zr. These elements were selected in terms of the potential stability of their oxides under the Deacon reaction conditions as discussed before.^[22] Criteria for stability were bulk chlorination and metal chloride volatilization temperatures, each of which should be higher than 500°C .

The normalized HCl conversion X_N after 4 h on stream plotted against that after 28 h on stream is shown in Figure 1. Between 4 and 28 h on stream, the HCl conversion of undoped

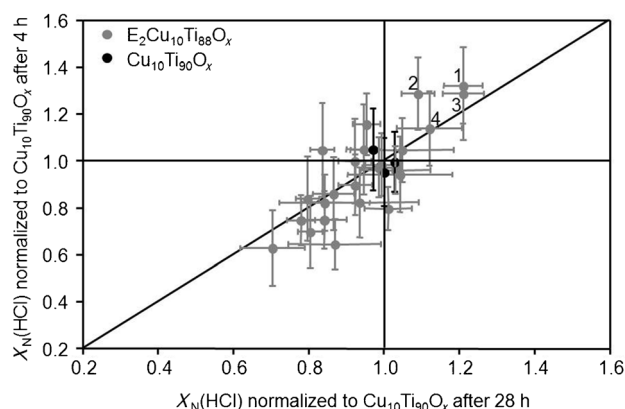


Figure 1. Conversion of $\text{E}_2\text{Cu}_{10}\text{Ti}_{88}\text{O}_x$ after 4 h on stream versus 28 h on stream; the HCl conversions were normalized to the HCl conversion of the undoped catalyst $\text{Cu}_{10}\text{Ti}_{90}\text{O}_x$; Conditions: $T=380^\circ\text{C}$, flow rate 25 mL min^{-1} , gas composition $\text{HCl}/\text{O}_2/\text{Ar}/\text{N}_2=1:2:2:5$, catalyst mass 37.5 mg ($100\text{--}200 \mu\text{m}$)+ 150 mg quartz sand ($200\text{--}300 \mu\text{m}$); 1) $\text{Nb}_2\text{Cu}_{10}\text{Ti}_{88}\text{O}_x$, 2) $\text{Si}_2\text{Cu}_{10}\text{Ti}_{88}\text{O}_x$, 3) $\text{Ge}_2\text{Cu}_{10}\text{Ti}_{88}\text{O}_x$, 4) $\text{Ta}_2\text{Cu}_{10}\text{Ti}_{88}\text{O}_x$.

$\text{Cu}_{10}\text{Ti}_{90}\text{O}_x$ decreased by 13 %, which suggests catalyst corrosion. Furthermore, the increased conversion error bars, especially after 28 h on stream, indicate that the catalysts had not reached steady state. Important for the following discussion are the samples in the upper-right corner of Figure 1, that is, $\text{Nb}_2\text{Cu}_{10}\text{Ti}_{88}\text{O}_x$, $\text{Si}_2\text{Cu}_{10}\text{Ti}_{88}\text{O}_x$, $\text{Ge}_2\text{Cu}_{10}\text{Ti}_{88}\text{O}_x$, and $\text{Ta}_2\text{Cu}_{10}\text{Ti}_{88}\text{O}_x$, which convert more HCl than $\text{Cu}_{10}\text{Ti}_{90}\text{O}_x$ after 4 and 28 h on stream, indicative of improved activity and long-term stability. These four compositions were selected for further optimization by composition spreads in the low-dopant concentration range. For these composition spreads the amount of doping element was varied between 1, 2, and 4 mol% with a fixed Cu content of 10 mol%.

The measurement results of the four catalyst groups are summarized in Figure 2. The conversions X_N for the Ge-doped mixed oxides were independent of the Ge content after 4 and

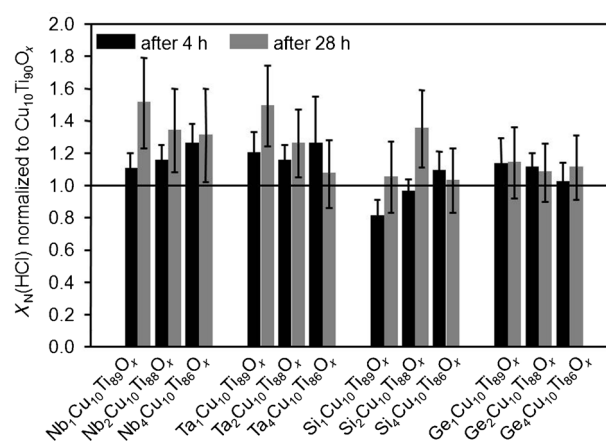


Figure 2. Variation of dopant amount for Nb, Ta, Si, and Ge in $\text{E}_2\text{Cu}_{10}\text{Ti}_{88}\text{O}_x$; Conversion of doped $\text{Cu}_{10}\text{Ti}_{90}\text{O}_x$ after 4 h on stream versus 28 h on stream; HCl conversions were normalized to the HCl conversion of the undoped catalyst $\text{Cu}_{10}\text{Ti}_{90}\text{O}_x$; Conditions: $T=380^\circ\text{C}$, flow rate 25 mL min^{-1} , gas composition $\text{HCl}/\text{O}_2/\text{Ar}/\text{N}_2=1:2:2:5$, catalyst mass 37.5 mg ($100\text{--}200 \mu\text{m}$)+ 150 mg quartz sand ($200\text{--}300 \mu\text{m}$).

28 h on stream. The best performing of the three silicon copper titanium oxides was $\text{Si}_2\text{Cu}_{10}\text{Ti}_{88}\text{O}_x$ after 28 h on stream, in contrast to the performance after 4 h on stream, for which 4 mol% Si was beneficial. The X_N gradients of the Nb- and Ta-doped oxides showed a similar trend, notably, after 28 h on stream. For both, 1 mol% doping resulted in the highest HCl conversions.

To validate the screening results, the STYs of $\text{Nb}_1\text{Cu}_{10}\text{Ti}_{89}\text{O}_x$, $\text{Ta}_1\text{Cu}_{10}\text{Ti}_{89}\text{O}_x$, and $\text{Ge}_1\text{Cu}_{10}\text{Ti}_{89}\text{O}_x$ were determined by iodometric titration after 28 h on stream (Table 1). The measured STYs confirmed the results of previous screening. $\text{Nb}_1\text{Cu}_{10}\text{Ti}_{89}\text{O}_x$ had

Catalyst	STY [$\text{g}_{\text{Cl}_2}\text{h}^{-1}\text{g}_{\text{catalyst}}^{-1}$]	Normalized $X_N(\text{HCl})$ ^[b]
$\text{Nb}_1\text{Cu}_{10}\text{Ti}_{89}\text{O}_x$	2.74	1.51
$\text{Ta}_1\text{Cu}_{10}\text{Ti}_{89}\text{O}_x$	2.68	1.49
$\text{Ge}_1\text{Cu}_{10}\text{Ti}_{89}\text{O}_x$	2.06	1.14
$\text{Cu}_{10}\text{Ti}_{90}\text{O}_x$	2.30	–

[a] Conditions: $T = 380^\circ\text{C}$, flow rate 25 mL min^{-1} , gas composition $\text{HCl}/\text{O}_2/\text{Ar}/\text{N}_2 = 1:2:2:5$, catalyst mass 37.5 mg ($100\text{--}200\text{ }\mu\text{m}$) + 150 mg quartz sand ($200\text{--}300\text{ }\mu\text{m}$). [b] Taken from Figure 2.

a slightly higher HCl conversion and STY than $\text{Ta}_1\text{Cu}_{10}\text{Ti}_{89}\text{O}_x$, so it was selected for the next generation.

Screening the second generation

As a result of the improvement of the chlorine yield achieved by the first-generation catalysts, the stabilization of Cu was the focus of the second generation. As dopants, the elements Al, Ca, Ce, Co, Ge, K, La, Mg, Na, Ni, Sc, Si, Sn, W, Y, and Zr (2 mol%) were selected. The reactions conditions of the second-generation screening ($T = 380^\circ\text{C}$, flow 25 mL min^{-1} , gas composition $\text{HCl}/\text{O}_2/\text{Ar}/\text{N}_2 = 1:2:2:5$) were identical to those of the first-generation screening. Apart from testing the catalytic activity, the Cu loss after 100 h on stream was used as indicator of catalyst stability. The amount of Cu in the mixed oxides before and after the Deacon reaction was determined by X-ray fluorescence spectroscopy (XRF). In this context, a linear relationship between the nominal Cu amount and XRF CuK_{α} signal intensity in the range from 2–12 mol% Cu could be confirmed experimentally for Nb-doped mixed oxides (Figure S1). Apart from Cu, the amount of other doping elements was also measured by XRF after the Deacon reaction, although the Ti content was not determined.

The results of the XRF analysis are shown in Table 2. The Ce-doped catalyst lost more than half of its Cu content over 100 h on stream. The most stable material was $\text{K}_2\text{Nb}_1\text{Cu}_{10}\text{Ti}_{87}\text{O}_x$, for which only 24% of the Cu was volatilized during the screening. The stabilizing effect of K on Cu-based Deacon catalysts is described in the literature^[16,28] and explained by the formation of the ternary chloride KCuCl_3 . KCuCl_3 lowers the melting point of the Cu compounds in the catalyst and affects the gas-phase

Table 2. Cu loss, dopant loss, and conversion X_N after 100 h on stream at $T = 380^\circ\text{C}$ of second-generation catalysts normalized to $\text{Nb}_1\text{Cu}_{10}\text{Ti}_{89}\text{O}_x$ ^[a]

Rank	Catalyst	Cu loss [mol %]	Dopant loss	$X_N(\text{HCl})$
1	$\text{K}_2\text{Nb}_1\text{Cu}_{10}\text{Ti}_{87}\text{O}_x$	24 ± 3	no loss	1.06 ± 0.05
2	$\text{Si}_2\text{Nb}_1\text{Cu}_{10}\text{Ti}_{87}\text{O}_x$	31 ± 2	not measurable	0.96 ± 0.10
3	$\text{Al}_2\text{Nb}_1\text{Cu}_{10}\text{Ti}_{87}\text{O}_x$	32 ± 2	not measurable	0.98 ± 0.07
4	$\text{Zr}_2\text{Nb}_1\text{Cu}_{10}\text{Ti}_{87}\text{O}_x$	35 ± 2	no loss	0.97 ± 0.03
5	$\text{Sn}_2\text{Nb}_1\text{Cu}_{10}\text{Ti}_{87}\text{O}_x$	36 ± 3	medium	1.00 ± 0.07
6	$\text{W}_2\text{Nb}_1\text{Cu}_{10}\text{Ti}_{87}\text{O}_x$	36 ± 2	no loss	0.80 ± 0.03
7	$\text{Mg}_2\text{Nb}_1\text{Cu}_{10}\text{Ti}_{87}\text{O}_x$	37 ± 2	not measurable	0.94 ± 0.07
8	$\text{Cu}_{10}\text{Ti}_{90}\text{O}_x$	37 ± 4	–	0.96 ± 0.12
9	$\text{Ge}_2\text{Nb}_1\text{Cu}_{10}\text{Ti}_{87}\text{O}_x$	39 ± 3	strong	1.00 ± 0.03
10	$\text{Cu}_{10}\text{Ti}_{90}\text{O}_x$	40 ± 4	–	0.91 ± 0.06
11	$\text{La}_2\text{Nb}_1\text{Cu}_{10}\text{Ti}_{87}\text{O}_x$	43 ± 2	slight	0.90 ± 0.03
12	$\text{Nb}_1\text{Cu}_{10}\text{Ti}_{89}\text{O}_x$	43 ± 2	–	1.02 ± 0.03
13	$\text{Na}_2\text{Nb}_1\text{Cu}_{10}\text{Ti}_{87}\text{O}_x$	44 ± 3	not measurable	0.98 ± 0.04
14	$\text{Ni}_2\text{Nb}_1\text{Cu}_{10}\text{Ti}_{87}\text{O}_x$	46 ± 2	no loss	1.06 ± 0.05
15	$\text{Sc}_2\text{Nb}_1\text{Cu}_{10}\text{Ti}_{87}\text{O}_x$	46 ± 4	slight	0.91 ± 0.06
16	$\text{Nb}_1\text{Cu}_{10}\text{Ti}_{89}\text{O}_x$	48 ± 3	–	0.98 ± 0.08
17	$\text{Co}_2\text{Nb}_1\text{Cu}_{10}\text{Ti}_{87}\text{O}_x$	48 ± 2	no loss	0.96 ± 0.08
18	$\text{Ca}_2\text{Nb}_1\text{Cu}_{10}\text{Ti}_{87}\text{O}_x$	48 ± 2	no loss	1.05 ± 0.08
19	$\text{Y}_2\text{Nb}_1\text{Cu}_{10}\text{Ti}_{87}\text{O}_x$	51 ± 3	no loss	0.84 ± 0.10
20	$\text{Ce}_2\text{Nb}_1\text{Cu}_{10}\text{Ti}_{87}\text{O}_x$	52 ± 3	slight	1.22 ± 0.07

[a] Conditions: flow rate 25 mL min^{-1} , gas composition $\text{HCl}/\text{O}_2/\text{N}_2 = 1:2:7$, catalyst mass 37.5 mg ($100\text{--}200\text{ }\mu\text{m}$) + 150 mg quartz sand ($200\text{--}300\text{ }\mu\text{m}$).

equilibrium between Cl_2 , CuCl , and CuCl_2 .^[28,29] This observation suggests that our catalyst is still affected by the bulk chlorination of Cu under the reaction conditions and that this Cu phase is stabilized by K. However, the effect of Na as a doping element was not as significant as that of K, an observation in line with the reports of Zhang et al. for Cu-based oxychlorination catalysts.^[30] Doping with Si, Al, and Zr was also beneficial for catalyst stability. Si and Al have already been reported as stabilizing elements for Ru-based catalysts.^[31,32]

The loss of doping elements was measured after a fixed reaction time. The two dopants Ge and Sn vaporized noticeably. Literature data suggest that GeO_2 should be stable against bulk chlorination.^[33] However, the hydration of GeO_2 to partially soluble H_4GeO_4 can also cause the observed leaching, which indicates that the water formed in the reaction causes corrosion effects. In the case of Sn-doped mixed oxides, SnCl_4 formed during the reaction,^[33] vaporizes at 380°C and hydrolyzes to SnO_2 .

Surprisingly, no correlation between Cu loss and conversion X_N was observed (Figure 3). The Ce-doped materials showed the highest Cu loss and conversion, whereas the Y-doped sample revealed an equal amount of Cu leaching but the lowest HCl conversion. Both, the K- and Ni-doped catalysts resulted in a normalized conversion X_N of 1.06, and the Ni-doped sample lost 46% of its Cu content, whereas the K-doped material only lost 24% of its Cu.

As no further improvement of the catalytic activity could be achieved and the dopants for stabilization were well known, we decided to focus entirely on the effect of Nb doping and the reaction conditions.

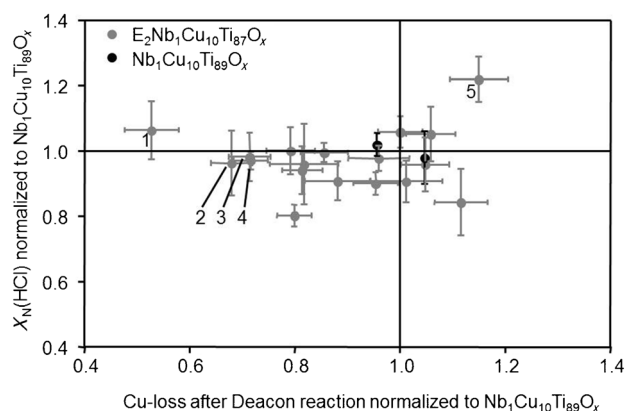


Figure 3. X_N plotted against Cu loss after 100 h on stream under Deacon reaction conditions with both axes normalized to $Nb_1Cu_{10}Ti_{89}O_x$. Conditions: $T=380^\circ\text{C}$, flow rate 25 mL min^{-1} , gas composition $\text{HCl}/\text{O}_2/\text{Ar}/\text{N}_2=1:2:2:5$, catalyst mass 37.5 mg ($100\text{--}200\text{ }\mu\text{m}$)+ 150 mg quartz sand ($200\text{--}500\text{ }\mu\text{m}$).

Influence of Nb doping level and O_2 partial pressure on Cu loss and STY

Amrute et al. and Farra et al. both showed the beneficial effects on the chlorine yield of an increased O_2 -to-HCl ratio for CeO_2 in the Deacon reaction.^[13,34] Therefore, we investigated the effect of the Nb doping level and O_2 partial pressure on the chlorine yield in the Deacon reaction of (Nb)CuTi mixed oxide samples by using a 2^2 factorial design. Two catalyst samples, one without (–) and one with (+) Nb, were tested during variations of the amount of O_2 between 20 (–) and 40 vol% (+) with a fixed HCl volume fraction of 10% in the feed. The impact of the O_2 partial pressure and the Nb doping level on the STY and Cu loss is characterized by the calculated effects [effect = average (+) levels – average (–) levels] and is shown in Tables 3 and 4. The dependence of one factor on the other is described as interaction.

Table 3. Factorial design and factor effects of the O_2 partial pressure and Nb doping level on the STY.

Experiment	O_2 partial pressure	Nb doping level	Interaction	STY [$\text{g}_{\text{Cl}_2}\text{ h}^{-1}\text{ g}_{\text{catalyst}}^{-1}$]
1	–	–	+	2.8
2	+	–	–	3.1
3	–	+	–	3.0
4	+	+	+	3.2
Effect	0.25	0.15	–0.05	

Table 4. Factorial design and factor effects of O_2 partial pressure and Nb doping level on Cu loss after 100 h on stream.

Experiment	O_2 partial pressure	Nb doping level	Interaction	Cu loss [%]
1	–	–	+	38.5
2	+	–	–	42.0
3	–	+	–	45.0
4	+	+	+	35.0
Effect	–4.25	–1.25	–7.75	

The STY increased with both increasing O_2 partial pressure and Nb doping level (Table 3). However, no interaction between both parameters was observed for chlorine production. On the other hand, the absolute value of the interaction parameter calculated from the Cu loss data for $Nb_1Cu_{10}Ti_{89}O_x$ (Table 4) is comparatively high. Notably, the lower the loss of Cu the more negative are the effects. A significant reduction of the Cu leaching can only be achieved by increasing both parameters, O_2 partial pressure and Nb doping level. These results are in accordance with results on a CeO_2 catalyst. The catalyst performance of CeO_2 in the Deacon reaction is related to the oxygen vacancies.^[13,34] In the case of Nb, apart from Nb_2O_5 and NbO_2 , there are five different stable Nb oxide phases, which are rich in oxygen vacancies and other defects.^[35,36] Accordingly, by doping Nb into our CuTi mixed oxide, the number of oxygen vacancies can increase. This increase of vacancies should promote chlorine production and enhanced stability in analogy to CeO_2 catalysts.

Activity and long-term stability

The HCl conversions of $\text{Cu}_{10}\text{Ti}_{90}\text{O}_x$ and $\text{Nb}_1\text{Cu}_{10}\text{Ti}_{89}\text{O}_x$ were determined by iodometric titration and are compared to that of a delafossite-type CuAlO_2 reference catalyst in Figure 4. The solid line in Figure 4 represents the equilibrium conversions calculated from data reported by Arnold and Kobe^[37] at the specified reaction conditions. It can be seen that across the whole temperature range, the Nb-doped catalyst is more active than the undoped catalyst. At $T=290^\circ\text{C}$, chlorine production of all samples was negligible. The HCl conversion of $\text{Nb}_1\text{Cu}_{10}\text{Ti}_{89}\text{O}_x$ at 380°C was 48%, and the material almost reached equilibrium conversions at 410°C . Although $\text{Cu}_{10}\text{Ti}_{90}\text{O}_x$ converted 39% HCl at $T=380^\circ\text{C}$, equilibrium conversion was reached not before 440°C .

For the long-term tests, the O_2 content of the feed was increased to 40 vol% and the delafossite-type sample was used as a reference. Delafossite-type CuAlO_2 has been reported to survive over 1000 h on stream without significant deactivation or leaching.^[17] In close agreement with this data reported by Mondelli et al. in Ref. [17], an activation of CuAlO_2 was observed during the first 50 h (Figure 5a). However, the CuTi mixed oxide catalysts prepared by a sol-gel method produced five times more Cl_2 than the delafossite-type reference catalyst (Figure 5b). The specific surface area of our CuAlO_2 sample calcined at 1100°C was too small to be analyzed by BET measurements. For the catalysts prepared by a sol-gel method, however, no correlation between the specific surface area and STY was found (see catalyst characterization section). After 100 h on stream, the relative STY of $\text{Nb}_1\text{Cu}_{10}\text{Ti}_{89}\text{O}_x$ and $\text{Cu}_{10}\text{Ti}_{90}\text{O}_x$ decreased from 2.9 to 2.2 and from 2.8 to $1.8\text{ g}_{\text{Cl}_2}\text{ h}^{-1}\text{ g}_{\text{catalyst}}^{-1}$, respectively.

After 25 h on stream, the Cu content of delafossite-type CuAlO_2 remained nearly constant up to the end of the experiments after 100 h, whereas the Cu content of the CuTi catalysts decreased continuously over the whole test duration. The

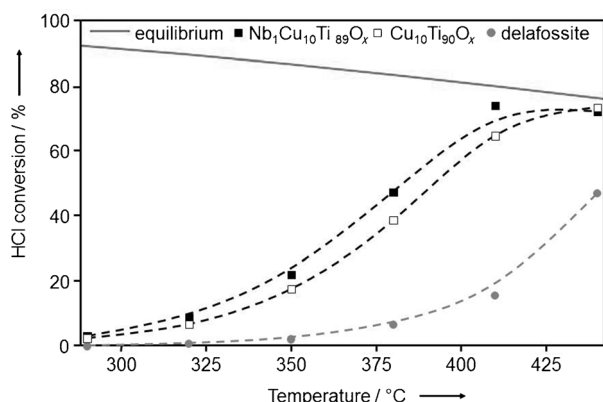


Figure 4. Light-off curves for $\text{Cu}_{10}\text{Ti}_{90}\text{O}_x$, $\text{Nb}_1\text{Cu}_{10}\text{Ti}_{89}\text{O}_x$, and delafossite-type CuAlO_2 ; Conditions: flow rate 25 mL min^{-1} , gas composition $\text{HCl}/\text{O}_2/\text{N}_2 = 1:2:7$, catalyst mass 37.5 mg ($100\text{--}200\text{ }\mu\text{m}$)+ 150 mg quartz sand ($200\text{--}300\text{ }\mu\text{m}$).

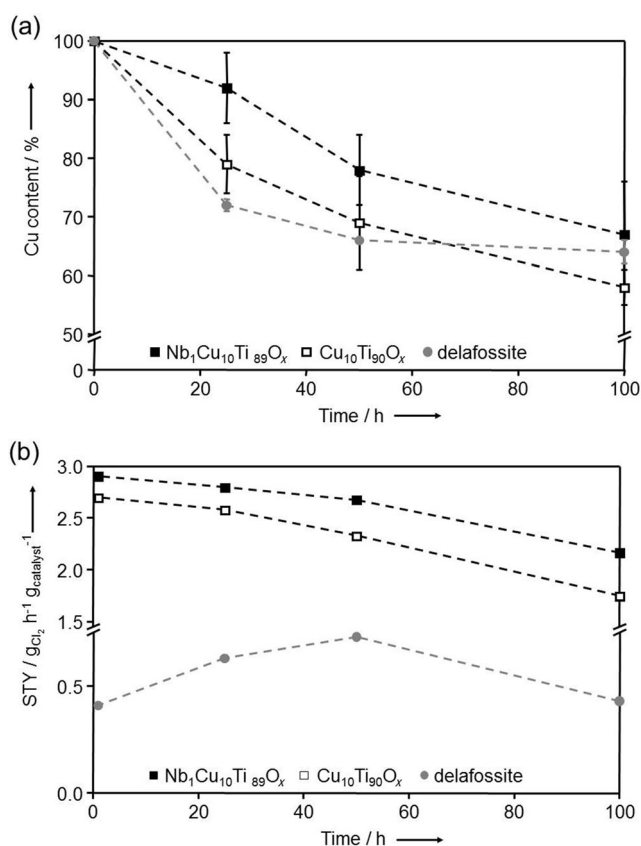


Figure 5. a) Cu loss versus time; b) STY versus time on stream; Conditions: $T = 380^\circ\text{C}$, flow rate 25 mL min^{-1} , gas composition $\text{HCl}/\text{O}_2/\text{N}_2 = 1:2:7$, catalyst mass 37.5 mg ($100\text{--}200\text{ }\mu\text{m}$)+ 150 mg quartz sand ($200\text{--}500\text{ }\mu\text{m}$).

Nb-doped catalyst lost 35% less Cu than the pure CuTi mixed oxide catalyst, which lost 45% of its Cu. Although increasing the Nb content to 4 mol% did not lead to higher stability (the Cu loss was also 35%), during the first 50 h of the reaction Nb doping stabilized the Cu phase (lower Cu loss, lower STY decrease). Thereafter, both materials lost constant amounts of Cu and activity. Thus, the Nb doping affects not only the chlorine

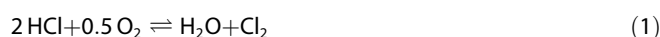
yield of the Cu catalyst but it also stabilizes the active phase. In contrast to the findings for other catalysts by Over and Schomäcker, CuO cannot be stabilized by excess O_2 only,^[38] and our results suggest that additional stabilizing strategies such as doping with Nb, K, Si, Al, or a combination of these as well as bringing Cu into a stable crystal structure, such as CuCrO_2 , are essential.^[18]

Finally, we observed solid deposition by sublimation or gas-phase transport in the colder reactor parts. They changed their color from yellow-brown to white with a shade of green immediately after reaction in contact with air, which indicates the transition of water-free CuCl_2 into CuCl_2 hydrate. The formation of CuCl_2 was also validated by XRF. The Cu/Cl ratio measured was 35:65 ($\text{Nb}_1\text{Cu}_{10}\text{Ti}_{89}\text{O}_x$) and 39:61 ($\text{Cu}_{10}\text{Ti}_{90}\text{O}_x$), which is close to the theoretical ratio of 33:67 for CuCl_2 .

Kinetic model parameters

As our aim was to identify the dependence of the reaction rate on the reactants and products with high accuracy, which requires a material with long-term stability, we selected reaction conditions with excess O_2 at a molar ratio of at least $\text{O}_2/\text{HCl}/\text{N}_2 = 3:1:4$ for this purpose. This initial O_2 partial pressure of 0.38 bar guaranteed an oxidizing atmosphere for the catalyst that avoids bulk chlorination and the evaporation of copper chloride from the catalyst. In a detailed study on the effect of excess oxygen it was shown that increasing oxygen in the feed gas significantly reduced Cu leaching, confirming the catalyst stabilization at high O_2 partial pressure (see Table 4).^[24] Within the investigated conditions, the apparent HCl reaction order was determined from differential measurements to be 0.13, whereas that of O_2 was 0.44 (Figure 6a). This means that both reactants show a positive, though for HCl only slight, influence on the reaction rate. However, both products (Cl_2 and H_2O) strongly chemisorb to the catalyst and inhibit the reaction as the strongly bent curves of reaction rates determined as a function of residence time reveal (Figure 6c). This observation implies that the rates shown in Figure 6a were not determined under ideal differential conditions as the measured conversion varies with feed composition, and thus this effect leads to an underestimation of the influence of the reactant pressures on the reaction rate, expressed by the unusually low reaction orders. The importance of H_2O and Cl_2 chemisorption on Cu-based catalysts was also observed in temporal analysis of products (TAP-2) experiments.^[25]

Based on the stoichiometric equation [Eq. (1)], the rate of the reaction can be expressed with the formal kinetic rate law [Eq. (2)]:



$$r = (k_f p_{\text{O}_2}^{0.44} p_{\text{HCl}}^{0.13} - \frac{k_f}{K p_{\text{O}_2}^{0.05} p_{\text{HCl}}^{1.87}} p_{\text{Cl}_2}^1 p_{\text{H}_2\text{O}}^1) / (1 + K_{\text{Cl}_2} p_{\text{Cl}_2} + K_{\text{H}_2\text{O}} p_{\text{H}_2\text{O}}) \quad (2)$$

in which k_f is the forward rate constant and K is the equilibrium constant equal to the square root of the thermodynamic

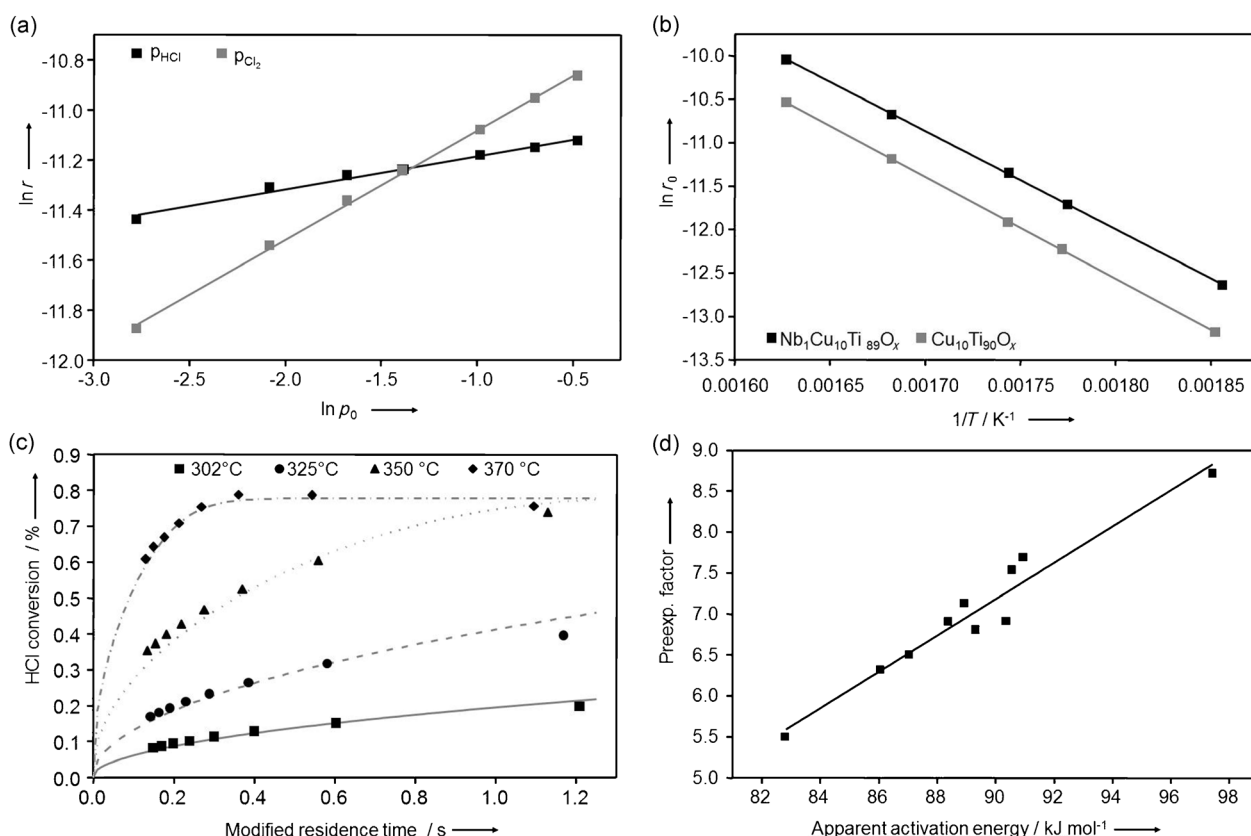


Figure 6. The influence of a) HCl and O₂ partial pressure and b) temperature on the reaction rate at 300 °C and 1 bar in the Deacon reaction over Nb₁Cu₁₀Ti₈₉O_x. c) The reactor temperature is increased from 300 to 370 °C in a residence-time variation with a feed of O₂ and HCl in a molar ratio of 3:1 with 50% dilution with N₂. d) Constable–Cremer correlation of Arrhenius parameters obtained from experiments between 300 and 370 °C and conversions between 10 and 70%.

equilibrium constant [Eq. (3)]:

$$K = \frac{p_{\text{Cl}_2} p_{\text{H}_2\text{O}}}{p_{\text{HCl}}^2 p_{\text{O}_2}^{0.5}} = \sqrt{K_{\text{Deacon}}} \quad (3)$$

in which K_{Cl_2} and $K_{\text{H}_2\text{O}}$ are the inhibition constants of chlorine and water, respectively. The denominator represents the usual inhibition term, and the numerator includes the derived rate dependences on the reactant partial pressures. The complex reverse rate coefficient ensures that the rate goes to zero at equilibrium pressure conditions. The apparent activation energy estimated from initial rates without the co-feed of a product in the temperature range of 300–370 °C is 94 kJ mol⁻¹, which is slightly decreased compared to the undoped Cu catalyst (Figure 6b). A weaker temperature dependence is expected if inhibition effects are caused by the products at a higher conversion level. The determination of the temperature dependence of the reaction at higher conversions shows a strong variation of the Arrhenius parameters, which are correlated according to the Constable–Cremer relationship (Figure 6d). This reflects a substantial change of the catalyst surface with the composition of the reaction gas. With increasing partial pressure of chlorine, the catalyst surface is increasingly more chlorinated and, therefore, changes its catalytic performance, as shown for a Ru catalyst by using a surface-sensi-

tive scattering method.^[39] With increasing temperature, the product inhibition effects decrease. From the temperature dependence of the inhibition term, a desorption enthalpy of 110 kJ mol⁻¹ can be estimated. At 300 °C, the inhibition constants are in the range of 10³ bar⁻¹. As chlorine and water are always produced in equimolar ratios, the assignment of this value to one of the products is only possible from experiments with additional product feed. The derived kinetic parameters are average values, which are only valid under the investigated experimental conditions. For the given conditions, the pre-exponential factor of the forward rate constant k_f is $5 \times 10^8 \text{ bar}^{0.43} \text{ g}^{-1} \text{ s}^{-1}$. For an exact description of the catalyst performance in a broad range of process conditions, coverage-dependent kinetic parameters would be required, which can only be determined with an enormous experimental effort.

Catalyst characterization

Specific surface areas (S_{BET}) and pore size distributions were determined by N₂ sorption experiments. Representative adsorption and desorption isotherms of a Ti oxide prepared by the sol–gel method are shown in Figure 7. The surface and pore size distribution of all materials are summarized in Table 5. Doping with 10 mol% Cu tripled the BET surface area. In addition, Nb doping increased the surface area. The increase of po-

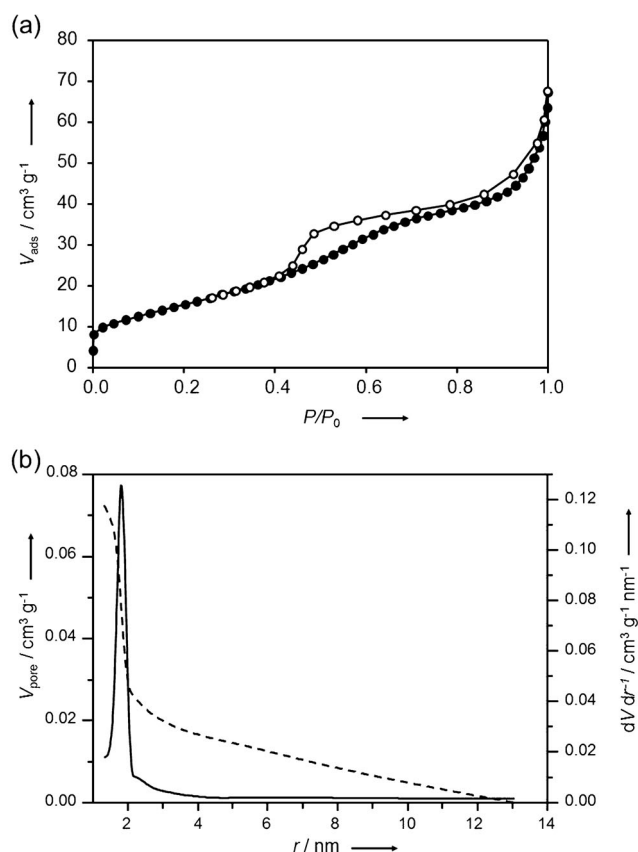


Figure 7. Adsorption and desorption isotherms (left) and pore radius distribution calculated by the BJH method (right) of $\text{Ti}_{100}\text{O}_x$.

rosity and surface area is a common phenomenon of mixed oxides, especially if prepared by using mild sol-gel approaches.^[40] As a result of the statistical mixed oxide structure, single-phase formation is hampered and amorphous microstructures tend to form preferentially.

If we changed the ageing conditions during catalyst synthesis (ageing in a Petri dish instead of a 20 mL beaker), the pore size distribution shifted to higher radii. However, the specific surface area also decreased, but without affecting the STY. This observation confirmed the suggestion of Pan et al. and Wolf et al. that during the Deacon reaction the active phase of

many transition metal salts is liquid and spreads over the carrier surface, especially for Cu-based catalysts.^[41,42]

The diffraction patterns of $\text{Cu}_{10}\text{Ti}_{90}\text{O}_x$ and $\text{Nb}_1\text{Cu}_{10}\text{Ti}_{89}\text{O}_x$ before and after 100 h under Deacon reaction conditions revealed only a single anatase phase (Figure 8). For the verifica-

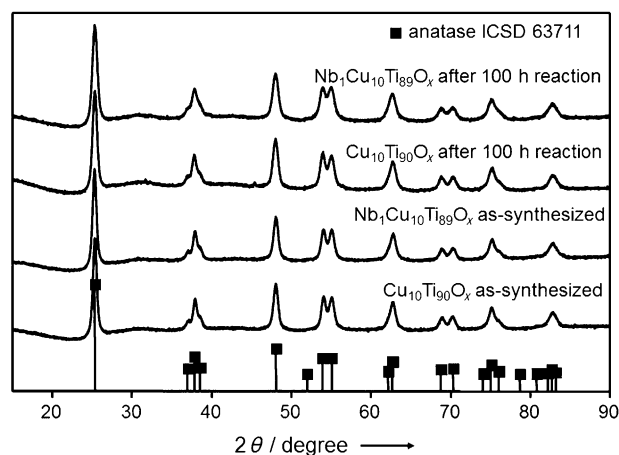


Figure 8. XRD patterns of $\text{Cu}_{10}\text{Ti}_{90}\text{O}_x$ and $\text{Nb}_1\text{Cu}_{10}\text{Ti}_{89}\text{O}_x$ as synthesized and after 100 h on stream. Vertical lines with black squares mark calculated anatase-type TiO_2 diffraction reflections from ICSD data set no. 63711.

tion of the incorporation of dopant elements into the crystal lattice of anatase-type TiO_2 , Rietveld refinement of the diffraction patterns of freshly prepared samples was performed, which were expected to reveal lattice parameter changes compared to the undoped reference catalyst TiO_2 (Table 6). If we doped TiO_x with Cu, the average crystallite size L decreased

Table 6. Lattice parameters and crystallite size of undoped and doped anatase-type TiO_2 after preparation. The standard deviations for the last number indicated from Rietveld refinements are given in parentheses.

	Crystallite size L [nm]	Lattice parameter [Å]	
		a	c
$\text{Ti}_{100}\text{O}_x$	38.1(4)	3.785(1)	9.493(1)
$\text{Cu}_{10}\text{Ti}_{90}\text{O}_x$	11.5(1)	3.783(1)	9.489(1)
$\text{Nb}_1\text{Cu}_{10}\text{Ti}_{89}\text{O}_x$	23.2(3)	3.786(1)	9.492(1)

Table 5. STY dependence on BET surface areas and pore size radii achieved by variation of sol-ageing conditions for $\text{Ti}_{100}\text{O}_x$, $\text{Cu}_{10}\text{Ti}_{90}\text{O}_x$ and $\text{Nb}_1\text{Cu}_{10}\text{Ti}_{89}\text{O}_x$.^[a]

	Sol-ageing procedure	STY	BET surface area [m ² g ⁻¹]	N ₂ sorption	
		[g _{Cl₂} h ⁻¹ g _{catalyst} ⁻¹]		Mean pore radius ^[b] [nm]	Max. pore radius ^[b] [nm]
$\text{Ti}_{100}\text{O}_x$	20 mL beaker	–	58		
$\text{Cu}_{10}\text{Ti}_{90}\text{O}_x$	20 mL beaker	2.8	179	2.0	2.0
$\text{Nb}_1\text{Cu}_{10}\text{Ti}_{89}\text{O}_x$	20 mL beaker	2.9	209	1.8	1.8
$\text{Cu}_{10}\text{Ti}_{90}\text{O}_x$	Petri dish	2.8	90	2.5	2.5
$\text{Nb}_1\text{Cu}_{10}\text{Ti}_{89}\text{O}_x$	Petri dish	3.1	97	2.5	2.5

[a] Conditions: $T=380^\circ\text{C}$, flow rate 25 mL min⁻¹, gas composition $\text{HCl}/\text{O}_2/\text{N}_2=1:2:7$, catalyst mass 37.5 mg (100–200 μm)+150 mg quartz sand (200–500 μm). [b] Pore radius determined by using the BJH method.

from 38.1 to 11.5 nm, which indicates crystal growth complicated by the dopant. Additionally, the lattice parameters a and c of anatase also decreased slightly but almost insignificantly if we consider the standard deviations. If Cu^{2+} or Cu^{1+} ions substitute for Ti^{4+} ions in the lattice, one might argue that the unit cell parameters increase because of the larger ionic radii of 0.77 and 0.73 Å of $\text{Cu}^{1+/2+}$ ions compared

to the Ti^{4+} ion (0.605 Å; all radii for coordination number CN = 6).^[43] However, for electroneutrality reasons this substitution is accompanied either by the occupation of interstitial lattice positions (e.g., Cu^{2+} replaces Ti^{4+} plus Cu^{2+} on interstitial sites) or by vacancy generation in the anionic partial lattice (e.g., Cu^{2+} replaces Ti^{4+} plus an O^{2-} vacancy), therefore, this argument might also fail. In the latter case both effects, increased cationic radii and vacancy formation, might compensate for each other to result in almost unchanged or even decreased lattice parameters. Welsch et al. observed an increase of the lattice parameter a in monoclinic MoO_2 caused by doping with Cu, the crystal structure of which is a distortion variant of the rutile type.^[44] As substitution effects depend on specific crystal structure features, this argument has to be considered again as not very powerful. As additional Cu-containing phases were not observed, overall there are no arguments against the assumption of the substitutional incorporation of Cu ions into the anatase crystal lattice.

Conclusion and Outlook

In this paper, a 10-fold parallel ageing reactor was successfully combined with a 10-fold sequential reactor to screen catalysts with long-term stability under the corrosive reaction atmosphere of the Deacon reaction at elevated temperatures. High-throughput technologies have been applied to optimize catalyst performance and lifetime. $\text{Nb}_1\text{Cu}_{10}\text{Ti}_{89}\text{O}_x$ was the catalyst with the highest Cl_2 space time yield in this study. Kinetic measurements revealed that Nb doping decreased the apparent activation energy. Additionally, a beneficial influence of the O_2 partial pressure on the reaction rate was observed in the kinetic experiments. Under oxidizing conditions with excess O_2 , 1 mol% Nb doping decelerated the Cu loss of the mixed-metal oxide and thus enhanced the catalyst lifetime. Additional stabilization was also achieved by doping $\text{Nb}_1\text{Cu}_{10}\text{Ti}_{89}\text{O}_x$ with K, Si, or Al. As a result of the high catalytic activity even at temperatures below 350 °C (the sublimation temperature of CuCl), we assume that the catalyst lifetime can be enhanced by decreasing the process temperature and still have an acceptable chlorine production even if the reaction rate is limited by product inhibition at low temperatures. Furthermore, it is possible that the stabilization effect of Nb can be extended to rutile-based catalysts as NbO_2 crystallizes in the rutile structure. However, first the mechanism of stabilization must be better understood, for which advanced catalyst characterization will be applied.

Experimental Section

Syntheses of CuTi catalysts

An alkoxide sol–gel route was used to synthesize the Ti-based materials.^[45] For example, $\text{Cu}_{10}\text{Ti}_{90}\text{O}_x$ (1 mmol) was prepared by mixing isopropyl alcohol (551 µL) with titanium(IV) isopropoxide (900 µL, 1 M solution in isopropyl alcohol) and copper(II) nitrate (1000 µL, 0.1 M in methanol) in the described order. Subsequently, the blue solution was stirred for 1 h. The sol was allowed to gel and dried for 7 d at RT. Finally the xerogel was calcined for 5 h at 400 °C (heating rate 0.5 °C min⁻¹).

For the doping, alcoholic solutions (0.1 M) of nitrates (Al, Ca, Ce, Co, K, La, Mg, Na, Ni, Y), chlorides (Sn, W), alkoxides (Ge, Nb, Ta, Ti), and nitrate oxide (Zr) were used. As the oxidation states of the metal ions in catalysts may vary with temperature and O_2 partial pressure during the different experimental stages of preparation, catalyst pretreatment, or under reaction conditions, the oxidation states of the prepared mixed-metal oxides are unknown and thus not specified. The materials are labeled by the amount of metal in mol% as a subscript. This means that the mixed-metal oxide $\text{Cu}_{10}\text{Ti}_{90}\text{O}_x$ consists of 10 mol% Cu and 90 mol% Ti.

Synthesis of delafossite-type CuAlO_2

For the synthesis of delafossite-type CuAlO_2 ,^[17] Al_2O_3 (Alfa Aesar) and Cu_2O (ZChL) were ground by using a laboratory ball mill. The homogenized mixture was calcined for 30 h at 1100 °C (heating rate 10 °C min⁻¹). The resulting solid was ground again by using the ball mill and calcined for 30 h at 1100 °C (heating rate 10 °C min⁻¹).

Catalytic testing

The setup for catalytic testing has already been described in detail.^[22,23] Catalytic testing was conducted in a sequential 10-fold reactor equipped with a mass spectrometer for online gas analysis. The reaction gases HCl , O_2 , Ar, and N_2 were dispensed by mass flow controllers. N_2 was also used for dilution of the process gas at the reactor outlet down to the injection valve of the mass spectrometer and to flush the whole setup after the experiment. By using a 10-port selector valve upstream to the reactor block, the gas flow through each plug flow reactor was controlled. The 10 glass reactor tubes (inner diameter 3 mm) were arranged in a circular Al heating block so that they were all the same distance from the central heating cartridge. The process off-gas was directed through a custom-made unit of backpressure valves machined from Inconel alloy 625, which avoided back-mixing between the separate reactors. The gas injection to the MS was software controlled by an electric four-port two-position valve. To limit the loading of the MS filament with corrosive gases, every 20 min the process gas was sampled for 30 s. In the remaining time the device was flushed with N_2 . To prevent water condensation, all lines and valves after the reactor outlets were heated to 110 °C. The complete testing process was automated through the software LabView.

Each reactor was loaded with catalyst (37.5 mg, sieve fraction 100–200 µm) diluted with quartz sand (75 or 150 mg, sieve fraction 200–300 µm). The reaction gas mixture was $\text{HCl}/\text{O}_2/\text{Ar}/\text{N}_2$ 1:2:2:5 at a weight hourly space velocity (WHSV) of 40 000 mL g⁻¹ h⁻¹. Ar was used as an internal standard for MS analysis. The process gas analysis was performed by using a quadrupole MS QMA 200 supplied by Pfeiffer Vacuum Corp. using one blank reactor as a bypass for internal calibration.

For better comparison of each reaction run, the calculated HCl conversions of all catalysts were normalized (X_N = normalized HCl conversion) to a $\text{RuO}_2/\text{SnO}_2$ reference catalyst supplied by Bayer MaterialScience or alternatively to the undoped $\text{Cu}_{10}\text{Ti}_{90}\text{O}_x$.

The STY of the catalysts, determined by MS, was validated by iodometric titration. The sample was taken manually by passing the process gas through 100 mL of 0.1 M KI solution for a predefined time (1–4 min). A portion of this sample (25 mL) was transferred to a potentiometric titrator 888 Titrand from Metrohm Corp.

Catalyst ageing

Catalyst ageing was performed in the parallel 10-fold fixed-bed reactor. A major problem of parallel fixed-bed reactors is to maintain identical gas flows through each reactor tube, which require identical pressure resistances. Pressure resistance may vary with different catalyst beds because of packing, particle size distributions, bed lengths, or constructional reactor geometry differences. This potential problem was solved here by the use of flow capillaries, the pressure resistances of which were significantly larger than those of the catalyst beds. Therefore, ten capillaries of optimized lengths and thus flow resistances were used to ensure identical gas flows (Figure S2). To confirm the accuracy of the setup, a catalytic test with two different catalysts each split into five reactors was carried out under Deacon reaction conditions (Figure S3). After the reactors, the process gases were collected in the common outlet and absorbed in caustic soda solution. The reactors were placed in a brass heating block similar to the sequential 10-fold reactor assembly. The catalyst loading and WHSV for each channel was identical to those of the catalytic testing.

Kinetic investigation

For steady-state kinetic measurements, the catalyst was first powdered by ball milling. A sieve fraction of 200–280 μm sized particles was prepared and 1 g of it was diluted with 4 g glass beads and mixed well to minimize the occurrence of hot spots in the reactor. An atmospheric pressure reactor operated at $T=300^\circ\text{C}$ was fed with a range of reactant gas mixtures by using mass flow controllers, and Cl_2 formation was quantified by iodometric titration. The catalytic tube reactor was made of silica glass with 8 mm inner diameter. Various reaction feed compositions with a total flow of 80 mL min^{-1} were used to evaluate the formal kinetic dependence of the reaction rate to the reactants and products (for more details see Ref. [46]). The partial pressures of the reactants were varied in the range of 0.0625–0.5 bar. The conversion level was always below 10% to allow kinetic evaluation. By calculating the Knudsen diffusion coefficient and the Wheeler–Weisz modulus, it was verified that the reaction was not limited by intraparticle diffusion.

Catalyst characterization

The amount of Cu in the samples was analyzed by X-ray fluorescence line intensity analysis by using an Eagle μ -Probe II spectrometer from EDAX (supplied by Roentgenanalytik Systeme GmbH). The catalyst powders were ground and pressed to tablets. The intensity of the CuK_α line was determined at four different surface positions on each tablet. The average of these four measurements provided the amount of Cu specified in the tables.

N_2 physisorption experiments were performed by using a Carlo Erba Sorptomatic 1990 at $T=-197^\circ\text{C}$. The samples were degassed at 200°C for 2 h (heating rate 5°C min^{-1}). The specific surface and the pore size distribution were determined by the BET^[47] and the Barret–Joyner–Halenda (BJH) method.^[48]

Powder XRD patterns were measured by using a PANalytical X'pert Pro MPD diffractometer with Ni-filtered Cu radiation [$\lambda(\text{CuK}_\alpha)=1.5418\text{ \AA}$] in reflection mode. The lattice parameters were determined by full profile Rietveld refinement by using TOPAS software.^[49]

Acknowledgements

This work was supported by the German “Bundesministerium für Bildung und Forschung” (BMBF) under contact number 033R018G.

Keywords: chlorine • copper • niobium • sustainable chemistry • titanium

- [1] EUROCHLOR: The European Chlor-Alkali Industry: An Electricity Intensive Sector Exposed to Carbon Leakage, http://www.eurochlor.org/media/9385/3-2-the_european_chlor-alkali_industry_an_electricity_intensive_sector_exposed_to_carbon_leakage.pdf, accessed 07.02.2012.
- [2] J. Pérez-Ramírez, C. Mondelli, T. Schmidt, O. F. K. Schlüter, A. Wolf, L. Mleczko, T. Dreier, *Energy Environ. Sci.* **2011**, *4*, 4786–4799.
- [3] A. Hiroyuki, U. Youhei, K. Seki, C. Knapp, O. Norihito, K. Masahiro, *Sumitomo Kagaku* **2010**, 1–10.
- [4] T. Hibi, H. Nishida, H. Abekawa (Sumitomo Chemical), EP 0743277A1, **1996**.
- [5] O. Osaka-shi, K. Iwanaga, T. Suzuta, Y. Mori, M. Yoshii (Sumitomo Chemical), EP 1170250A1, **2002**.
- [6] A. Wolf, L. Mleczko, O. F. K. Schlüter, S. Schubert (Bayer MaterialScience), US 2007/0274897A1, **2007**.
- [7] A. Wolf, L. Mleczko, S. Schubert, O. F. K. Schlüter (Bayer MaterialScience), US 2007/0274901, **2007**.
- [8] A. Wolf, J. Kintrup, O. F. K. Schlüter, L. Mleczko (Bayer MaterialScience), US 2007/0292356A1, **2007**.
- [9] H. Over, *J. Phys. Chem. C* **2012**, *116*, 6779–6792.
- [10] H. Over, *Chem. Rev.* **2012**, *112*, 3356–3426.
- [11] E. V. Kondratenko, A. P. Amrute, M.-M. Pohl, N. Steinfeldt, C. Mondelli, J. Pérez-Ramírez, *Catal. Sci. Technol.* **2013**, *3*, 2555–2558.
- [12] A. P. Amrute, C. Mondelli, T. Schmidt, R. Hauert, J. Pérez-Ramírez, *ChemCatChem* **2013**, *5*, 748–756.
- [13] A. P. Amrute, C. Mondelli, M. Moser, G. Novell-Leruth, N. López, D. Rosenthal, R. Farra, M. E. Schuster, D. Teschner, T. Schmidt, J. Pérez-Ramírez, *J. Catal.* **2012**, *286*, 287–297.
- [14] Y. Tozuka, *Stud. Surf. Sci. Catal.* **1995**, *92*, 41–50.
- [15] A. P. Amrute, C. Mondelli, J. Pérez-Ramírez, *Catal. Sci. Technol.* **2012**, *2*, 2057–2065.
- [16] F. Wattimena, W. M. H. Sachtler, *Stud. Surf. Sci. Catal.* **1981**, *7*, 816–827.
- [17] C. Mondelli, A. P. Amrute, T. Schmidt, J. Pérez-Ramírez, *Chem. Commun.* **2011**, *47*, 7173–7175.
- [18] A. P. Amrute, G. O. Larrazábal, C. Mondelli, J. Pérez-Ramírez, *Angew. Chem.* **2013**, *125*, 9954–9957; *Angew. Chem. Int. Ed.* **2013**, *52*, 9772–9775.
- [19] H. F. Johnstone, *Chem. Eng. Prog.* **1948**, *44*, 657–668.
- [20] A. P. Amrute, F. Krumeich, C. Mondelli, J. Pérez-Ramírez, *Chem. Sci.* **2013**, *4*, 2209–2217.
- [21] V. E. Tarabanko, N. V. Tarabanko, N. V. Koropachinskaya, *Catal. Ind.* **2010**, *2*, 259–265.
- [22] M. Hammes, M. Valtchev, M. B. Roth, K. Stöwe, W. F. Maier, *Appl. Catal. B* **2013**, *132–135*, 389–400.
- [23] Parallel fixed-bed microreactors for high-throughput screening with special focus on high corrosion resistance and new Deacon catalysts for chlorine production: K. Stöwe, M. Hammes, M. Valtchev, M. Roth, W. F. Maier, in *Modern Applications of High Throughput Experimentation in Heterogeneous Catalysis* (Ed.: A. Hagemeyer, A. Volpe), Bentham Science, eBook Chapter, in press.
- [24] M. Hammes, Dissertation, Saarland University, **2013**.
- [25] A. P. Amrute, C. Mondelli, M. A. G. Hevia, J. Pérez-Ramírez, *J. Phys. Chem. C* **2011**, *115*, 1056–1063.
- [26] J. W. Saalfrank, W. F. Maier, *Angew. Chem.* **2004**, *116*, 2062–2066; *Angew. Chem. Int. Ed.* **2004**, *43*, 2028–2031.
- [27] K. Hachmeister, *Z. Anorg. Allg. Chem.* **1919**, *109*, 145–186.
- [28] B. Neumann, *Angew. Chem.* **1915**, *28*, 233–236.
- [29] C. M. Fontana, E. Gorin, G. A. Kidder, C. S. Meredith, *Ind. Eng. Chem.* **1952**, *44*, 363–369.

- [30] T. Zhang, C. Troll, B. Rieger, J. Kintrop, O. F. K. Schlüter, R. Weber, *Appl. Catal. A* **2009**, *365*, 20–27.
- [31] K. Seki, *Catal. Surv. Asia* **2010**, *14*, 168–175.
- [32] C. Mondelli, A. P. Amrute, F. Krumeich, T. Schmidt, J. Pérez-Ramírez, *ChemCatChem* **2011**, *3*, 657–660.
- [33] Y. Ivashentsev, V. I. Ivantsova, *Russ. J. Phys. Chem.* **1969**, *43*, 505–508.
- [34] R. Farra, M. Eichelbaum, R. Schlögl, L. Szentmiklósi, T. Schmidt, A. P. Amrute, C. Mondelli, J. Pérez-Ramírez, D. Teschner, *J. Catal.* **2013**, *297*, 119–127.
- [35] H. Schäfer, D. Bergner, R. Gruehn, *Z. Anorg. Allg. Chem.* **1969**, *365*, 31–50.
- [36] T. Kikuchi, M. Goto, *J. Solid State Chem.* **1976**, *16*, 363–371.
- [37] C. W. Arnold, K. A. Kobe, *Chem. Eng. Prog.* **1952**, *48*, 293–296.
- [38] H. Over, R. Schomäcker, *ACS Catal.* **2013**, *3*, 1034–1046.
- [39] D. Teschner, G. Novell-Leruth, R. Farra, R. Schlögl, H. Soerijanto, R. Schomäcker, N. López, *Nat. Chem.* **2012**, *4*, 739–745.
- [40] G. Frenzer, W. F. Maier, *Annu. Rev. Mater. Res.* **2006**, *36*, 281–331.
- [41] H. Y. Pan, R. G. Minet, S. W. Benson, T. T. Tsotsis, *Ind. Eng. Chem. Res.* **1994**, *33*, 2996–3003.
- [42] F. Wolf, F. Runge, R. Korn, *Z. Anorg. Allg. Chem.* **1960**, *304*, 48–57.
- [43] R. D. Shannon, *Acta Crystallogr. Sect. A* **1976**, *32*, 751–767.
- [44] F. G. Welsch, K. Stöwe, W. F. Maier, *ACS Comb. Sci.* **2011**, *13*, 518–529.
- [45] C. Lettmann, H. Hinrichs, W. F. Maier, *Angew. Chem.* **2001**, *113*, 3258–3262.
- [46] D. Teschner, R. Farra, L. Yao, R. Schlögl, H. Soerijanto, R. Schomäcker, T. Schmidt, L. Szentmiklósi, A. P. Amrute, C. Mondelli, J. Pérez-Ramírez, G. Novell-Leruth, N. López, *J. Catal.* **2012**, *285*, 273–284.
- [47] S. Brunauer, P. H. Emmett, E. Teller, *J. Am. Chem. Soc.* **1938**, *60*, 309–319.
- [48] E. P. Barrett, L. G. Joyner, P. P. Halenda, *J. Am. Chem. Soc.* **1951**, *73*, 373–380.
- [49] TOPAS, General Profile and Structure Analysis Software of Powder Diffraction Data, v2.1, Bruker AXS; Karlsruhe, Germany, **2003**.

Received: August 20, 2013

Published online on November 5, 2013